Structural characterization of aluminium alloy 7075–graphite composites fabricated by mechanical alloying and hot extrusion

R. Deaquino-Lara, E. Gutiérrez-Castañeda, I. Estrada-Guel, G. Hinojosa-Ruiz, E. García-Sánchez, J.M. Herrera-Ramírez, R. Pérez-Bustamante, **R. Martínez-Sánchez**

Abstract

The modification on the microstructure and mechanical response of some Al7075–graphite composites fabricated by mechanical alloying and hot extrusion were studied as a direct function of milling time (0–10 h) and graphite concentration (0–1.5 wt.%). The experimental results show that the mechanical properties of the resulting composites are enhanced by increasing both the milling time and the graphite content. This effect is attributed mainly to grain size refining, Al4C3 phase formation and an increase of the dislocation density. The yield strength of the hot-extruded samples varies with grain size according to the Hall–Petch relationship. During the hot-extrusion process, recrystallization of samples milled for 10 h occurs faster than in samples with 5 h of milling, which is associated to the increase of stored energy in the composites caused by the milling process.

1. Introduction

Aluminium is considered as the second most used metal in the world. Due to its high formability, lightweight, high electrical conductivity and corrosion resistance, it has many applications. Recently, there exists an increasing interest in producing high-strength and lightweight components aimed mainly for aerospace and automotive applications. This represents a motivation to study and develop new materials that can satisfy this demand.

Aluminium–matrix composites (AMC) are materials, in which Al or its alloys are strengthened by dispersion of hard particles like carbides (Al4C3, SiC, TiC), oxides (Al2O3) or nitrides (TiN, AlN) into the matrix. These reinforcement particles also increase wear resistance, high-temperature strength and refractoriness, making them attractive for the applications mentioned above.

Several methods have been reported to synthesize these materials including pressure-less infiltration [1], squeeze casting [2] ; [3], semi-solid mechanical stirring [4] and recently, mechanical alloying (MA). The latter is a simple and useful technique to produce aluminium matrix composites and consists of repeated flattening, cold welding, fracturing, and rewelding of a mixture of powder particles in a high-energy ball mill. This technique offers some advantages such as: (a) fine and homogeneous distribution of the alloying elements and the reinforcing particles in the matrix, avoiding segregation of the reinforcement, which is a typical problem presented in the casting processes and (b) microstructure refining to nanometric levels: enabling the production of nanostructured materials in a relative short time and at the same time produces a large amount of lattice defects (vacancies, dislocations, grain boundaries), which can improve the diffusion and incorporation of alloying elements into the metallic matrix in order to form a solid solution [5]. The diffusion of elements into the metal matrix is a well-known process commonly observed during the mechanical milling [6]; [7] ; [8]. All of the phenomena mentioned above, result in superior properties when compared with materials fabricated by casting methods.

It has been reported that graphite can be used as reinforcement for Al-

composites produced by mechanical milling increasing the strength of these materials [9]; [10]; [11] ; [12]. Other researchers have found that additions of graphite nanoparticles causes an increase of the ultimate tensile strength (UTS) and hardness of 7075 aluminium alloys up to 40% and 20%, respectively [9].

The hardening effect of the graphite particles (G) is related to the fact that mechanical milling (MM) produces grain refining and favors the homogeneity of graphite-particles dispersion. In addition, the presented graphite in the matrix reacts with Al and forms Al4C3 during the sintering and hot extrusion processes [6]; [10]; [11] ; [12] according to the chemical reaction $4Al + 3C \rightarrow Al_4C_3$. The formation of this phase contributes to the increase of the composites strength due to its small size (~100 nm) and its high hardness (1000–1400 HV), working as a barrier to the dislocation motion. As the amount of this phase increases, the composite strength also increases. Al4C3 is one of the reinforced-agents commonly used to fabricate Al–matrix composites, however, the effects of graphite additions on the microstructural evolution and mechanical properties of Al7075alloys have been scarcely studied.

The present investigation is focused in studying the effects of milling time and the graphite content on the microstructure and mechanical properties of aluminium–graphite composites synthesized by MA and hot extrusion.

2. Experimental procedure

The Al7075 composites were produced by mixing pure elemental powders of Al, Zn, Mg, Cu, Mn and G. The last one had a purity of 99.9% and an average particle size of 21 μm, whereas the rest of the components had purity of 90% and

particle sizes smaller than 51 μm. The graphite particles were produced by MM in a high-energy ball mill (SPEX-8000M). The milling time was set to 8 h and the selected atmosphere to avoid oxidation was argon. Table 1 lists the proportions of the raw powders used in this investigation.

Table 1
Chemical composition and sample identification used in this assignment.

Sample	Composition (wt.%)							
	Zn	Mg	Cu	Cr	Fe	Mn	G	Al
Al_{7075}-5Zn0.0G	5.1	2.5	1.6	0.23	0.30	0.20	0.0	90.07
Al_{7075}-5Zn0.5G							0.5	89.57
Al_{7075}-5Zn1.0G							1.0	89.07
Al_{7075}-5Zn1.5G							1.5	88.57

Composite mixtures were blended in the same equipment for 5 min without grinding balls in order to obtain homogeneous mixtures. Then, they were mechanically alloyed in a high-energy ball mill (Simoloyer CM-01) for 5 and 10 h under an argon atmosphere. In this way, the formation of the Al7075 alloy and the dispersion of graphite particles into the aluminium alloy matrix were achieved in the same process.

The milling device and the milling media were made from stainless steel. The milling ball-to-powder weight ratio was kept at 14:1, the weight for all of the samples was 70 g and methanol (3 ml) was used as a process control agent (PCA). Consolidated bulk products (40 mm in diameter) were obtained by pressing the milled powder under uniaxial load of ~950 MPa for 2 min. Then, the samples were sintered in vacuum during 3 h at 823 K using a heating rate of 50 K/min. Sintered products were held at 773 K and hot extruded into 10 mm-diameter bars by indirect extrusion with an extrusion ratio of 16. An additional sample in the as-mixed

condition (without milling and 0% G), but prepared by the same route, was employed as reference material (Al7075·5Zn0.0G–M).

The microstructure of the as milled powders and extruded samples was characterized by X-ray diffraction (XRD), scanning electron microscopy (SEM) and transmission electron microscopy (TEM). XRD analyses were performed in a Panalytical X'Pert PRO diffractometer (40 kV, 35 mA) with Cu Kα radiation (λ = 0.15406 nm). Observations by SEM and TEM were carried out in a JEOL JSM6510-LV (operated at 20 kV) and JEOL JEM2200F (operated at 200 kV), respectively. The samples used for TEM studies were prepared with the focused ion beam (FIB) lift-out technique [13] in a JEOL JEM-9320 FIB (operated at 30 kV).

The grain structure of the extruded samples was determined by the electron backscattered diffraction technique (EBSD) in a Philips SEMXL30 microscope equipped with a goniometer for texture measurements. Grain structure maps were obtained in a direction parallel to the extrusion direction on the bars surface. Finally, uniaxial tensile tests along the extrusion direction were carried out at room temperature in a MTS 810 universal testing machine, with an overhead displacement rate of 0.016 mm/s. The yield strength (σy) was determined with the 0.2% offset method based on ASTM: E-8 standard.

3. Results and discussion

3.1. Microstructure of the as-milled powders

Fig. 1 shows two SEM images of the Al7075–G composite obtained after milling. It is observed that the powder particles are agglomerated, exhibiting irregular shapes (similar to flakes) with different sizes. This is because during the milling

process of ductile materials, the powder particles are continuously welded and fractured as a result of the constant collisions between the milling media and powders. It is also clear that the particle size decreases as the milling time increases from 5 to 10 h; this is a typical characteristic of MM process. Each of these powder particles is constituted with a large amount of crystallites and its microstructure can be observed by TEM.

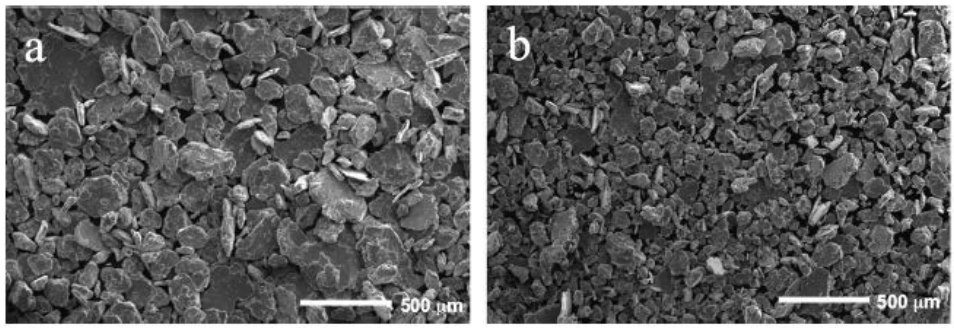

Fig. 1. SEM images showing morphological evolution of the Al_{7075}·5Zn1.0G powder composites, after (a) 5 h and (b) 10 h of milling.

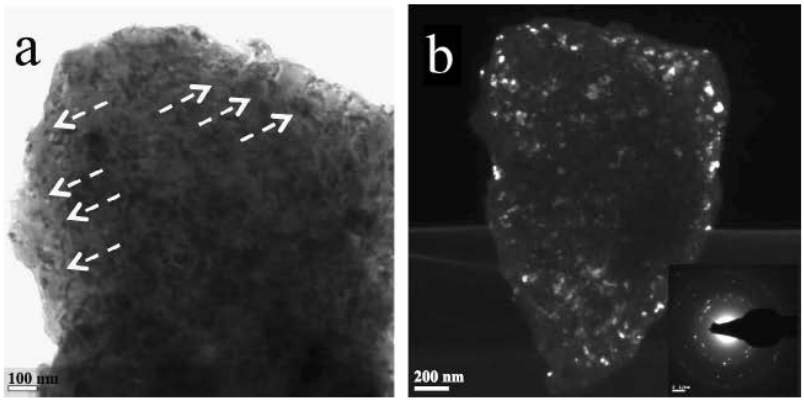

Fig. 2. TEM images of the as-milled Al_{7075}·5Zn0.5G powders composites after 10 h of milling, (a) bright-field and (b) dark-field showing the grain size in the powder particle.

Fig. 2 shows representative bright and dark field TEM images as well as the selective area diffraction (SAD) pattern corresponding to milled powders during 10 h (Al7075·5Zn0.5G). It is clearly observed that the final crystal size has decreased to

nanoscale range becoming a nanostructured material with grain size smaller than 50 nm. High-deformation zones are seen in the powder particles, dashed arrows, which have a high density of dislocations that were caused by the milling process [8].

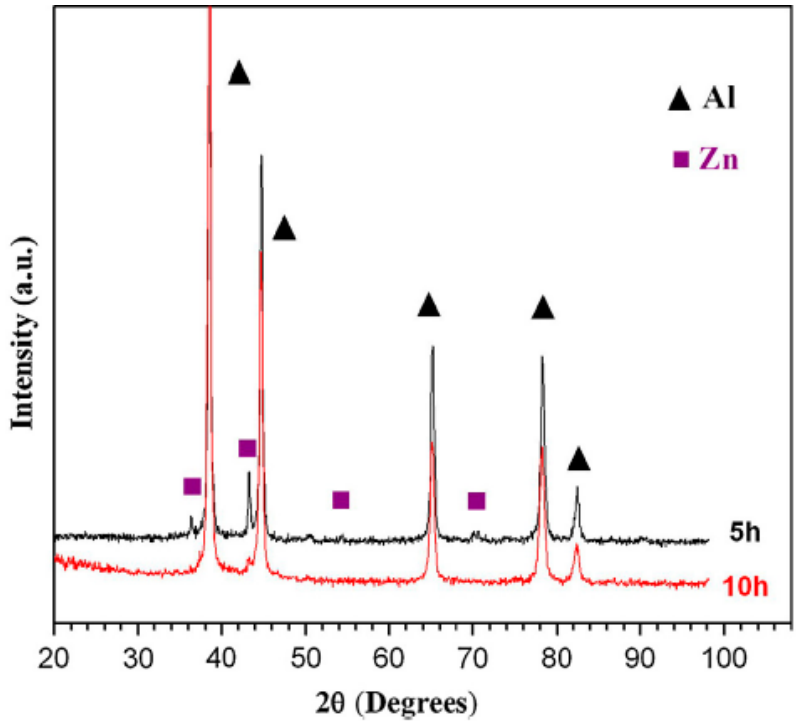

Fig. 3. XRD patterns of the Al_{7075} milled powders composites; the formation of other phases is not observed.

The Gibbs free energy (DGf) at the sintering temperature 823 K, needed to the formation of the aforementioned carbides, were cal-culated using some theoretical relationships reported in the litera-ture [15–19], which are expressions of DGf as a function of the temperature.

According to the results of Table 2, during sintering at 823 K the formation of Al4C3,Cr23C6 and Cr7C3 is thermodynamically possi-ble, being more spontaneous the Al4C3 formation. In contrast, the formation of Fe3C at this temperature cannot

occur.

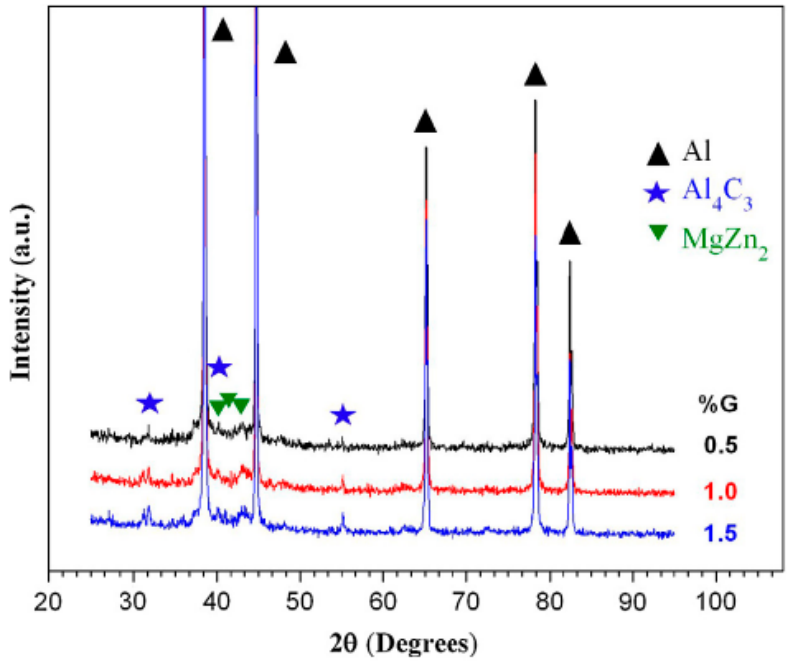

Fig. 4. XRD patterns of Al_{7075} extruded composites showing the formation of Al_4C_3 and $MgZn_2$ after hot extrusion.

The amount of chromium-based carbides should be very small due to the low concentration of Cr in the alloy; considering the possibility that some of them were formed during the heat treatment. Therefore, they would not have a significant effect on the mechanical properties of the alloy.

The presence of the aluminium carbide (Al4C3) was confirmed by TEM studies. Fig. 5 presents a TEM image showing the presence of the Al4C3 phase formed by a reaction between graphite and Al. According to the literature [6,20] the formation of this phase during mechanical alloying requires longer times than the ones used in this investigation. However, the formation of this phase is much

Table 2
Gibbs free energy calculated at 823 K.

Carbide	ΔG_f
Al_4C_3	−324.7 kJ/mol [15]
$Cr_{23}C_6$	−280.0 kJ/mol [16] −307.2 kJ/mol [17]
Cr_7C_3	−135.0 kJ/mol [16] −126.2 kJ/mol [17]
Fe_3C	2.1 kJ/mol [18] 4.2 kJ/mol [19]

Faster at temperatures between 673 and 723 K [11]. Therefore, graphite, which is well dispersed due to the milling process, reacts with aluminium crystallizing as Al4C3 during sintering and extrusion processes performed at 823 K.

The extruded samples were analyzed by TEM in order to observe the microstructural features of Al7075–G composites in a deeper way after the sintering and hot extrusion processes. Bright and dark field TEM images of the previously milled powders (Al7075-□5Zn0.0G) for 0, 5 and 10 h are shown in Fig. 6. It is clear that the grain size of samples without milling (Fig. 6a) is larger compared to that of samples previously milled for 5 and 10 h (Fig. 6b and c). The microstructure of the unmilled sample (0 h) shows evidence of the presence of some grains of about 3 lm, which is reduced to 1.5 lm and less than 1 lm after 5 h and 10 h of milling, respectively.

One of the limitations of TEM analyses is that the local area considered for the analysis is very small. Therefore, the observed microstructure could not be representative of the entire sample (it depends of the grain size homogeneity). The EBSD technique was used to evaluate the grain size distribution in the extruded samples in order to complement the TEM analysis. Fig. 7 shows the EBSD maps

obtained in samples presented in Fig. 6 (previously milled for 0, 5 and 10 h). As it can be observed, the grain size of extruded samples decreases significantly as the milling time in-creases. The microstructure not only shows the presence of large, deformed and elongated grains parallel to the extrusion direction

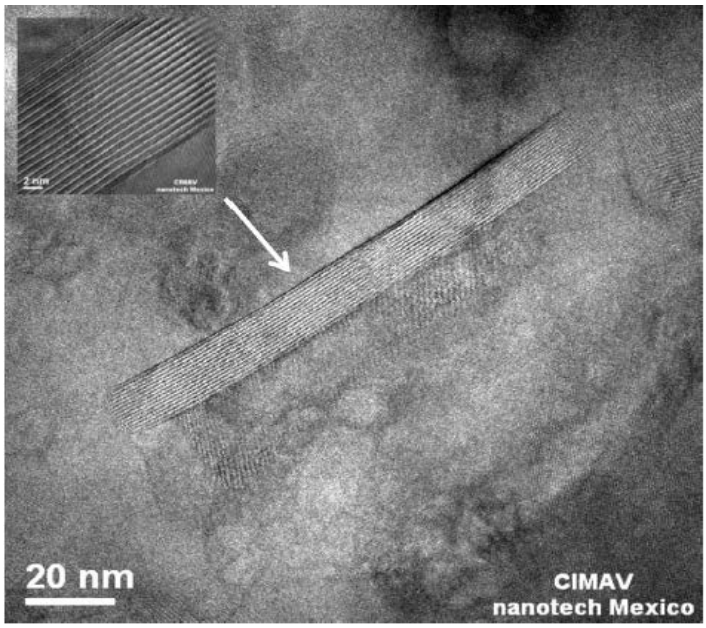

Fig. 5. TEM image showing the presence of Al_4C_3 in the Al matrix.

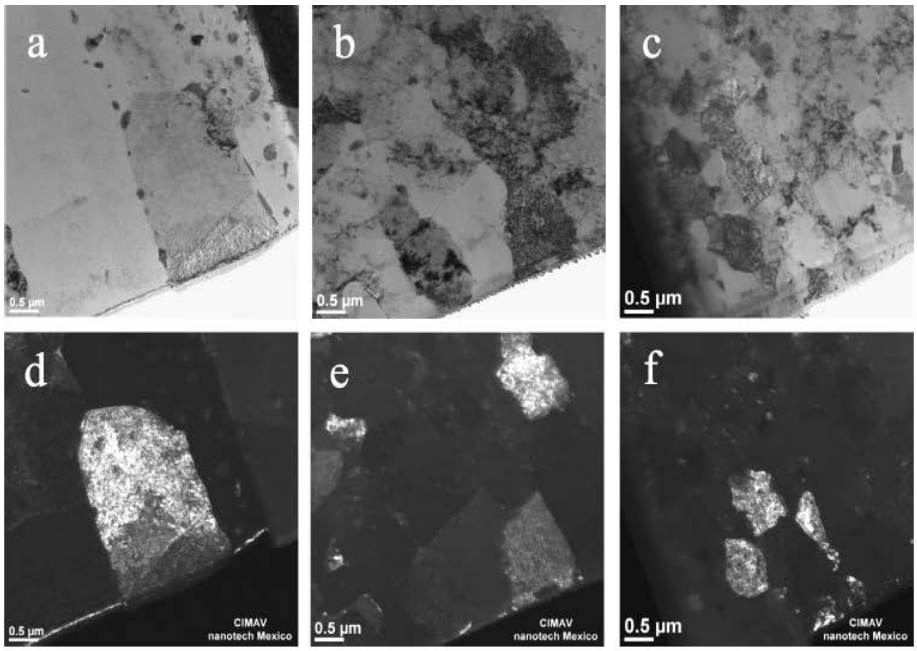

Fig. 6. TEM images (bright-field) of the as-extruded samples previously milled at: (a) 0 h, (b) 5 h and (c) 10 h, and the corresponding dark-field images: (d) 0 h, (e) 5 h and (f) 10 h.

(Fig. 7a) but also a wide distribution of sizes in unmilled samples. On the other hand, an almost recrystallized microstructure is observed after the hot extrusion processing in samples previously milled for 5 h (Fig. 7b). The results showed not only a more uniform microstructure but also smaller recrystallized grains and a lower distribution size (Fig. 7c) when the milling time were in-creased to 10 h.

Fig. 8 illustrates the mean grain diameter (MGD) as a function of the milling time. As it can be seen, the MGD was about 4 lm in un-milled samples, while it was reduced to 1.5 and 1 lm in samples milled for 5 and 10 h. Furthermore, the scattering bars indicate the high variability in grain size for the unmilled sample, compared with that of the other samples. It is very important to point out

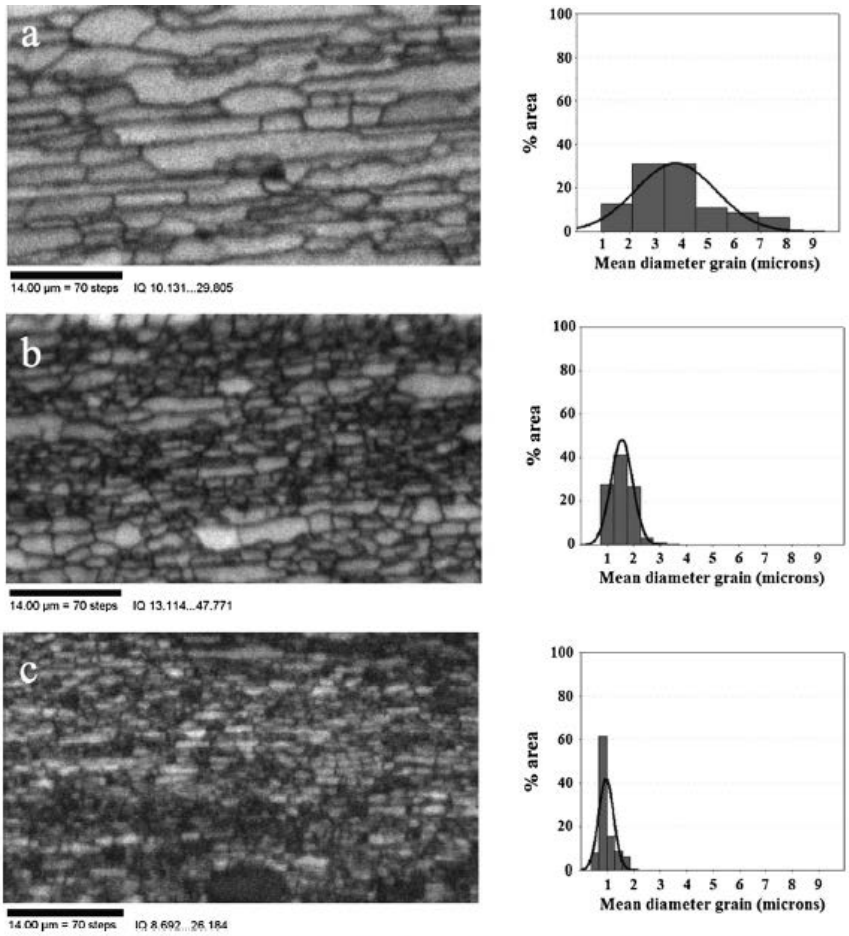

Fig. 7. EBDS maps showing the microstructure of the hot-extruded samples previously milled at: (a) 0 h, (b) 5 h and (c) 10 h, and their grain size distribution.

That the sample milled during 10 h exhibits some grains with sizes lesser than 1 lm. Nevertheless, they were not clearly visible at the magnification used for the analyses and, therefore, were not con-sidered for the measurements. Then, after 10 h of milling, the MGD of samples could be even much less than the reported value.

The recrystallization of the unmilled sample occurs slower than in samples previously milled for 5 and 10 h. It is known that the mechanical milling causes a reduction in the crystallite size and generation of lattice defects such as dislocations and vacancies [8]. These lattice defects are present in the material as stored en-ergy, which represents the driving force for the recrystallization process. Furthermore, these defects act as preferential sites for nucleation of the new grains during sintering and extrusion processes. As the amount of these defects during millings in-creases, the amount of sites for growing of new grains during ther-mal processes also increases. Then with a smaller crystallite size, the amount of lattice defects is higher and consequently the stored energy is also high [8, 21]. Thus, according to the obtained results, the unmilled sample has lower stored energy than those subjected to the milling process, which explains the retardation of the recrys-tallization process (Fig. 7a). Increasing the milling time causes an increase of the stored energy, accelerating the recrystallization;

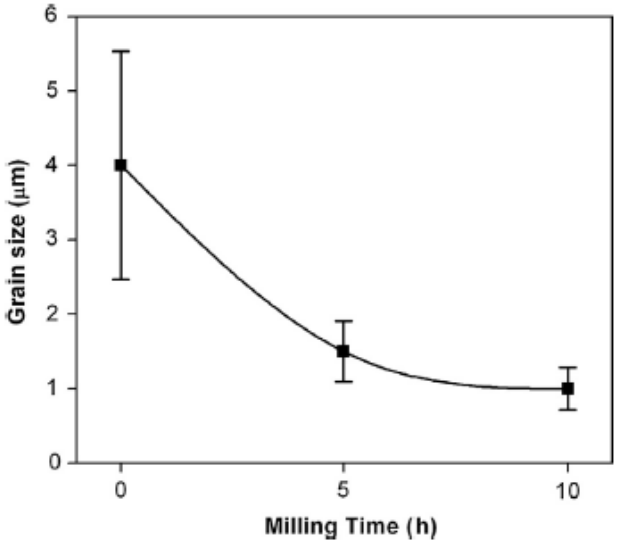

Fig. 8. The grain size of extruded samples from previously milled powders during 0, 5 and 10 h.

Mechanical properties of extruded composites as function of milling time and graphite content.

Sample	Milling time (h)	σ_y (MPa)	Variation (%)	σ_{max} (MPa)	Variation (%)	Vickers (μHV)	Variation (%)	Grain size (μm)
Al_{7075}-5Zn0GP-M	0	256.5	–	349.5	–	90.0	–	4
Al_{7075}-5Zn0.0GP	5	280.0	9.2	368.5	5.4	83.0	−7.8	1.6
Al_{7075}-5Zn0.5GP		265.5	3.5	330.0	−5.6	92.0	2.2	–
Al_{7075}-5Zn1.0GP		295.5	15.2	366.0	4.7	97.0	7.8	1.5
Al_{7075}-5Zn1.5GP		376.0	46.6	413.0	18.2	113.0	25.6	1.3
Al_{7075}-5Zn0.0GP	10	365.0	42.3	437.0	25.0	127.0	41.1	1
Al_{7075}-5Zn0.5GP		305.0	18.9	400.0	14.4	100.0	11.1	–
Al_{7075}-5Zn1.0GP		382.0	48.9	452.0	29.3	120.0	33.3	1
Al_{7075}-5Zn1.5GP		446.0	73.9	520.0	48.8	141.0	56.7	0.9
Al_{7075}-O	0	96.5	−62.4	221.0	−36.8	–	–	
Al_{7075}-T6		503.0	96.1	572.0	63.7	175.0	94.4	
Al_{7075}-T7		435.0	69.6	505.0	44.5	155.0	72.2	

3.3. Mechanical properties

The results of tensile tests obtained in extruded samples are shown in Table 3. As it can be seen, there is a significant increment in the yield strength (ry), UTS and Vickers microhardness (lHV) of the composites as the milling time and the graphite content in-crease. It can be observed in Table 3 that in the sample with 1.5 wt. % G and 5 h of milling (Al7075□5Zn1.5G), the yield strength (ry) increases up to

47% compared with the reference material (Al7075□5Zn0.0G–M). In the case of the samples milled for 10 h, the ry increases up to 19% and 74% with 0.5 and 1.5 wt.% G, respectively. A comparison between the mechanical properties of the composites and those reported in the literature for the Al7075 alloy in the O, T6 and T7 conditions is also presented in Table 3 [22].Asit can be observed, the mechanical properties of the composites are higher than those of the Al7075 in the annealed condition (O) and similar to those in the artificially aged condition (T73). Therefore, the mechanical properties of the composites synthesized can be improved with a subsequent heat treatment.

The enhancement on the mechanical properties observed in the composites was caused by different hardening mechanisms involved during processing: grain size refining, formation of Al4C3 phase, thermal mismatch between matrix and reinforcement particles, precipitation of MgZn2, dispersion of Al2O3 during the milling process, inhibition of dislocation motion by MgZn2,Al4C3, and Al2O3 nanoparticles. Because the precipitation of MgZn2 and dispersion of Al2O3 are very similar in all the composites, the only three important hardening mechanisms considered in this research are: grain size refining, formation of Al4C3 and an increment in the dislocation density (due to the thermal mismatch between Al–G and Al–Al4C3). In the former mechanism, it is observed that the grain size of milled powders decreases by increasing the milling time (Figs. 6–8); this reduction in the grain size results in an increment of the yield strength and UTS (Table 3). It is shown, in Fig. 9, that a smaller grain size means a higher ry value. Grain refining is a well-known hardening-mechanism in which dislocation motion is stopped by grain

boundaries that act as obstacles. Thus, the number of barriers to dislocation movement, and consequently the mechanical resistance, increases as the grain size decreases. This behaviour is in a good agreement with the dependence between yield strength and grain size described by the Hall–Petch relationship [23].

$$\sigma_y = \sigma_i + KD^{-1/2}$$

Where σ is the yield stress; ri the friction stress, representing the overall resistance of the crystal lattice to dislocation movement; K

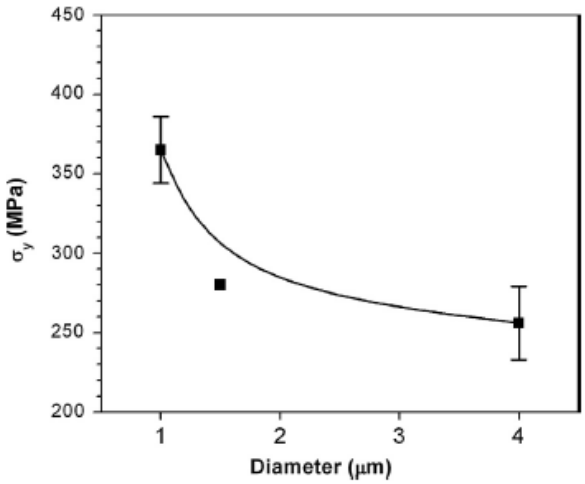

Fig. 9. Yield strength as a function of grain size.

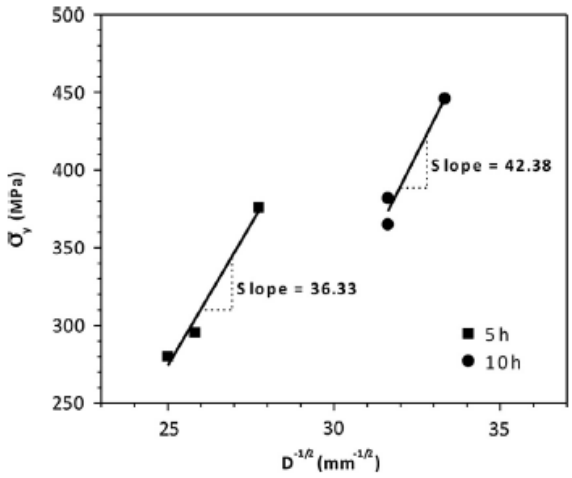

Fig. 10. r_y vs $D^{-1/2}$ plots obtained in samples with 5 and 10 h of milling.

The locking parameter, which measures the relative hardening con-tribution of the grain boundaries; and D is the grain size.

According to the results of Table 3, the yield strength of com-posites with 5 and 10 h of milling samples increases when the grain size decreases. Furthermore, as it can be observed in Fig. 10 there is a linear behaviour between ry and D□1/2. The results of

Table 4
Effect of milling time on K parameter in Hall–Petch equation.

Milling time (h)	K (MPa mm$^{1/2}$)	R^2
5	36.331	0.979
10	42.384	0.9604

Linear regression analysis presented in Table 4 shows that the strengthening effect of the grain boundary expressed by K in-creases by increasing the milling time. This behaviour shows the hardening effect due to the grain refining caused by mechanical milling.

Mechanical properties of composites are also affected by the graphite in two ways: the formation of Al4C3 and by thermal mismatch originated by heating and cooling during sintering and hot extrusion due to the difference of the expansion coefficients be-tween Al and G. The formation and dispersion evidence for this hard-phase (Al4C3) was presented in Figs. 4 and 5. The last Figure shows a higher magnification view (square inset) of the aluminium carbide dispersed in aluminium matrix. It is noticed that the width of the Al4C3 is around 20 nm. This carbide exhibits hard-ness between 1000 and 1400 HV [11], which is around 10–17 times higher than the hardness of the matrix (Table 3). It has been reported that the presence of

this carbide has an important hardening effect over the matrix due to the lattice distortion and probably to the fact that this crystallized phase works as a barrier to the dislocation movement [10–12]. Evidence of the interaction be-tween dislocations and Al4C3, which contributes with the increment of the strength observed, is presented in Fig. 11.

Nevertheless, not all of the graphite contained in the matrix re-acts with Al to form Al4C3, Fig. 12 illustrates a field-emission SEM image of a sintered and extruded composite with 1 wt.%G (Table 1), previously milled for 10 h. A graphite particle is observed, which exhibits an irregular shape and is completely embedded into the Al–matrix showing well-adherence to it. It is clearly observed that only a part of the available G reacts with Al to form the aluminium carbide and the unreacted G particles are visible in the Al–matrix.

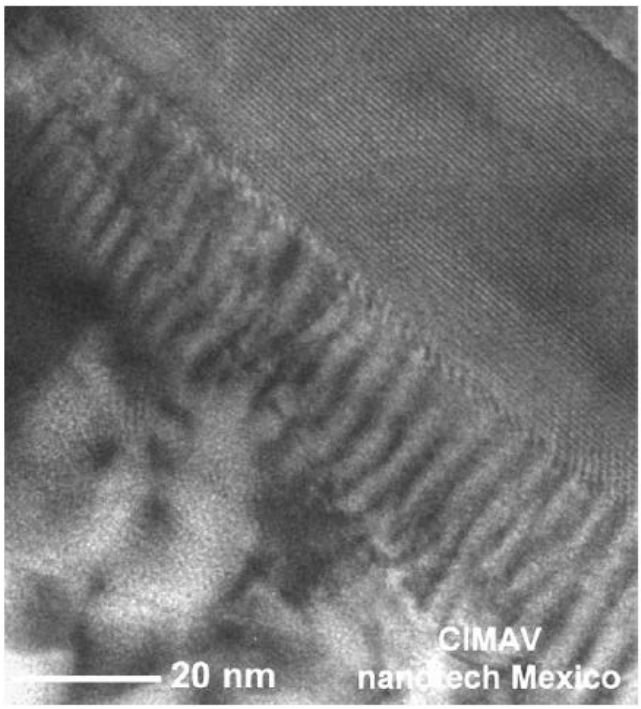

Fig. 11. Interaction of dislocations around aluminium carbide (Al_4C_3)

Then, the other way in which the G particles affect the mechanical properties of the composites is by the thermal mismatch, which produces an increment in the dislocation density between the matrix and the G particle [24,25]. The dislocation density (q due to the thermal mismatch can be represented with the following equation:

$$\rho = 8A\varepsilon/(bt(1-A))$$

Where A is the volume fraction of the reinforcement; e the thermal strain; b the Burger's vector and t is the smallest dimension of the particle.

It can be observed in this equation that the dislocation density is inversely proportional to the particle size. Thus, a smaller particle size results in an increase of the dislocation density. Besides, the relationship between dislocations and yield strength can be de-scribed as follows [24,25]:

$$\Delta\sigma_y = \alpha\mu b\rho^{1/2}$$

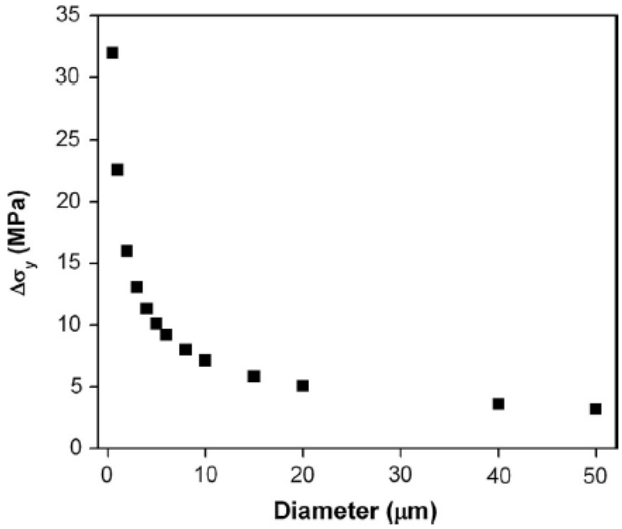

Fig. 13 as a function of the graphite particle size. Smaller particle size results in higher dislocation density and consequently higher yield strength.

where Dr is the increase in the yield strength, a the constant (1.25 for Al) [26], l the shear modulus (26 □ 103 MPa for Al), b the Burgers´s vector and q is the dislocation density. Fig. 13 shows a theoretical calculation of the yield strength as a function of graphite particles size in the range of the size of graphite powders initially added (0.5–50 lm). It is clearly observed that a smaller particle size produces higher yield strength. The unreacted graphite particles are expected to have a contribution to the composites strengthening between 20 and 30 MPa (Fig. 13) because they are in the range of 0.5–1.0 lm (Fig. 12). Thus, it can be summarized that the grain refining, formation and homogeneous dispersion of Al4C3 and the increment in the dislocation density are the main hardening mechanisms that contribute to the enhancement on the mechanical properties of the investigated composites.

4. Conclusions

Al7075–G composites were prepared by means of mechanical alloying; this method produced a notable grain refining and favored the incorporation of alloying elements and a homogeneous graphite dispersion. During the sintering and extrusion processes, added graphite reacted with Al and formed Al4C3, which contributed to the increment of the composites strength acting as a barrier to the dislocation motion. SEM, TEM and XRD evidence showed that the particle size of composites decreased during milling; with further processing the formation of nanostructured structures with grain size <50 nm were reached. Milling process induced the formation of uniform microstructures with smaller recrystallized grains and a thin distribution of particle sizes; even after the hot extrusion processing a tinny recrystallized microstructure was observed. The experimental results showed

that the mechanical response (strength and hardness) of composites increased as a direct function of the milling time and graphite content. The main hardening mechanisms associated with the processing route could be: grain size refining, formation of Al4C3 phase and the increment in the dislocation density. Based on these evidences, graphite addition followed by a solid state processing is an adequate route for the aluminium composites preparation, obtaining an increased mechanical response as a direct consequence of the highly refined microstructure and homogeneous distribution of reinforcement particles.

Acknowledgments

This research was supported by CONACYT under Grant No. 106658. Thanks to Red Temática de Nanociencias y Nanotecnología (Reg. 0124623) and Red Temática de Ciencia y Tecnología Espaciales (Reg. 0170962). The authors would gratefully thank K. Campos-Venegas, W. Antunez Flores, C. Ornelas Gutiérrez, E. Torres-Moyé, J.E. Ledezma Sillas, O. Solís Canto and Felipe Márquez for their valuable technical support through the study.

References

[1] Park WJ, Anowar Hossian MD, Choi YB, Park SH, Huh SC. A study on the manufacturing conditions of metal matrix composites by low pressure infiltration process. J Mech Sci Technol 2007;21:1694–9.

[2] Qu S, Geng L, Han J. SiCp/Al composites fabricated by modified squeeze casting technique. J Mater Sci Technol 2007;2007(23):641–4.

[3] Moosa AA, Al-Khazraji KK, Muhammed OS. Tensile strength of squeeze cast carbon fibers reinforced Al–Si matrix composites. J Miner Mater

Charact Eng 2011;2:127–41.

[4] Qin XH, Jiang DL, Dong SM. Nanometer, submicron and micron sized aluminum powder prepared by semi-solid mechanical stirring method with addition of ceramic particles. Mater Sci Eng A 2004;385:31–7.

[5] Ozdemir I, Ahrens S, Mucklich S, Wielage B. Nanocrystalline Al–Al2O3p and SiCp composites produced by high-energy ball milling. J Mater Process Technol 2008;205:111–8.

[6] Zhou Y, Li ZQ. Structural characterization of a mechanical alloyed Al–C mixture. J Alloys Compd 2006;414:107–12.

[7] Khina BB, Lovshenko GF. Modeling enhanced diffusion mass transfer in metals during mechanical alloying. In: Mohamed El-Amin (Ed.), Mass Transfer in Multiphase Systems and its Applications. InTech. ISBN: 2011; 978-953-307-

215- 9.

[8] Suryanarayana C. Mechanical alloying and milling. Prog Mater Sci 2001;46:1–184.

[9] Estrada-Guel I, Carreño-Gallardo C, Mendoza-Ruiz DC, Miki-Yoshida M, Rocha-Rangel E, Martínez-Sánchez R. Graphite nanoparticle dispersion in 7075 aluminum alloy by means of mechanical alloying. J Alloys Compd 2009;483:173–7.

[10] Bostan B, Özdemir AT, Kalkanli A. Microstructure characteristics in Al–C system after mechanical alloying and high temperature treatment. Powder Metall 2004;47:37–42.

[11] Besterci M. Preparation, microstructure and properties of Al–Al4C3 system produced by mechanical alloying. Mater Des 2006;27:416–21.

[12] Arik H. Production and characterization of in situ Al4C3 reinforced aluminum-based composite produced by mechanical alloying technique. Mater Des 2004;25:31–40.

[13] Giannuzzi LA, Stevie FA. A review of focused ion beam milling techniques for TEM specimen preparation. Micron 1999;30:197–204.

[14] Deaquino-Lara R, Estrada-Guel I, Hinojosa-Ruiz G, Flores-Campos R, Herrera-Ramírez JM, Martínez-Sánchez R. Synthesis of aluminum alloy 7075–graphite composites by milling processes and hot extrusion. J Alloys Compd 2011;509:S284–9.

[15] Qiu C, Metselaar R. Solubility of carbon in liquid Al and stability of A14C3.J Alloys Compd 1994;16:55–60.

[16] Kleykamp H. Thermodynamic studies on chromium carbides by the electromotive force (EMF) method. J. Alloys Compd 2001;1321:138–45.

[17] Anthonysamy S, Ananthasivan K, Kaliappan I, Chandramouli V, Vasudeva Rao PR, Mathews CK, et al. Gibbs energies of formation of chromium carbides. Metall Mater Trans A 1996;27:1919–24.

[18] Jang JH, Kim IG, Bhadeshia HKDH. First-principles calculations and the thermodynamics of cementite. Mater Sci Forum 2010;638–642:3319–24.

[19] Zhang YD, Esling C, Calcagnotto M, Gong ML, Zhao X, Zuo L. Shift of the eutectoid point in the Fe–C binary system by a high magnetic field. J Phys D Appl Phys 2007;40:6501–6.

[20] Wu NQ, Wu JM, Wang GX, Li ZZ. Amorphization in the Al–C system by mechanical alloying. J Alloys Compd 1997;260:121–6.

[21] Humphreys FJ, Hatherly M. Recrystallization and related annealing phenomena. 2nd ed. Oxford: Elsevier Ltd.; 2004.

[22] ASM Handbook, Properties and selection: Nonferrous alloys and special-purpose materials. 10th ed. ASM International: vol. 2, 1997.

[23] Dieter R. Mechanical metallurgy. 3rd ed. New York: McGraw-Hill; 1998.

[24] George R, Kashyap KT, Rahul R, Yamdagni S. Strengthening in carbon nanotube/aluminium (CNT/Al) composites. Scr Mater 2005;53:1159–63.

[25] Arsenault RJ, Shi N. Dislocation generation due to differences between the coefficients of thermal expansion. Mater Sci Eng 1986;81:175–87.

[26] Hansen N. The effect of grain size and strain on the tensile flow stress of aluminium at room temperature. Acta Metall 1977;25:863–9.